Journal of Materials Chemistry C

Thermal Phonon Mechanism of Amorphous AlN and Thermal Transport of Thin Amorphous Layers at the Interface

Journal:	*Journal of Materials Chemistry C*
Manuscript ID	TC-ART-09-2024-004157.R1
Article Type:	Paper
Date Submitted by the Author:	08-Feb-2025
Complete List of Authors:	Hwang, Taesoon; Seoul National University, Cho, Kyeongjae; The University of Texas at Dallas,

SCHOLARONE™
Manuscripts

ARTICLE

Thermal Phonon Mechanism of Amorphous AlN and Thermal Transport of Thin Amorphous Layers at the Interface

Received 00th January 20xx,
Accepted 00th January 20xx

DOI: 10.1039/x0xx00000x

Taesoon Hwang and Kyeongjae Cho*

AlN has received significant attention due to excellent thermal conductivity as a heat spreader for most modern electronic devices and next generation applications. AlN is usually deposited and fabricated as composites with many substrates (e.g., Si, Si_3N_4, SiC and Al_2O_3). In particular, the AlN film can have quite a high conductivity >100 $Wm^{-1}K^{-1}$, even though there is amorphous layer formation at the interface between AlN and substrates. However, the fundamental understanding of thermal property of amorphous AlN (a-AlN) layer has not been elucidated clearly. In this study, we examined thermal property of a-AlN. Thermal resistance (TR) of a-AlN thin layer (nm) is just few times higher than crystal AlN (c-AlN), while TR of bulk a-AlN is 100 × higher than TR of bulk c-AlN. Phonons of a-AlN consist of mainly diffuson that facilitate thermal transport well in the short range and phonon mean free path of a-AlN is 1.5 nm ~ 3nm in diffuson region. In addition, composite system of c-AlN/a-AlN/c-AlN with a-AlN layer less than 3nm thickness shows very small thermal transport reduction, which is comparable to pure c-AlN system, while there is continuously substantial increase in TR of the composite system with a-AlN layer over 3 nm thickness. In addition, the other electronic materials (e.g., Al_2O_3, GaN, SiC and Si_3N_4) have also mean free path within 3nm as good thermal bridge in amorphous phase. It means that the formation of amorphous thin layer at the interface of the different materials of hetero phases would be the thermal bridge.

Introduction

Thermal control has been the key precondition for the most electronic application such as high power, radio frequency (RF) electronics, high density integrated circuit and deep ultraviolet (UV) photonics.[1-5] The high power devices produce high joule heating and then cause high operating temperature impeding reliable performance and lifetime.[6,7] Some electronics shows the 2 × fast reduction in life time even at the 5°C increase compared to optimal temperature region.[7,8] For heat dissipation, many thermal conductive materials (e.g., Diamond, boron arsenide, aluminum nitride, gallium nitrite, graphene, silicon carbide) have been extensively studied for the last decade.[9]

In particular, AlN has received significant attention due to very large band gap of 6.1e V as well as high bulk thermal conductivity of 340 $Wm^{-1}K^{-1}$ at room temperature.[9-13] From the reasons, the thermal characteristic of bulk crystal AlN (c-AlN) has also been extensively examined as a promising material for thermal application in electronic devices. In addition, AlN generally shows good compatibility for heterogeneous integration with different materials (e.g., Si, and Al_2O_3), though bulk AlN shows different thermal properties depending on grain size, polycrystalline orientation, defects (e.g., oxygen contents), chemical and physical deposition conditions.[14-16]

The thermal conductivity of AlN film can reach the high thermal conductivity over than 100 $Wm^{-1}K^{-1}$, even though AlN film has the interfacial hetero junction with substrate.[16] In addition, the formation of thin amorphous layers at the interface frequently occurs. Nevertheless, the AlN film with amorphous layer shows high conductivity over than 100 $Wm^{-1}K^{-1}$ unlike that conventional understanding that amorphous phase has thermal conductivity of several orders of magnitude lower than crystalline crystal phase.[17] However, the fundamental mechanism of the amorphous AlN (a-AlN) thin layer in thermal transport and the application of thin amorphous layer for the thermal conduction have not been clearly elucidated yet. In addition, study on thermal property of amorphous structure has been complicated and limited in the view point of conventional understanding focusing on crystalline structure, because amorphous structures have difficulty to define well organized group velocity and harmonic oscillation.[18] The phonon properties for vibrational modes in amorphous structures rapidly vary, indicating different behavior from conventional phonon traveling of plane wave motions.[19]

For these reasons, we used density functional theory (DFT) and non-equilibrium Green's function formalism (NEGF) to investigate phonon transport of thin layer of amorphous and crystalline phase of AlN. In addition, lattice dynamics (LD) and molecular dynamics (MD) were also utilized to examine thermal properties of the amorphous materials based on modal analysis and spectrally decomposed heat

Department of Materials Science and Engineering, University of Texas at Dallas, Richardson, Texas 75080, United States.
**Corresponding author (E-mail: kjcho@utdallas.edu.)*
†Electronic Supplementary Information (ESI) available: Process of Melt-Quenching method, Phonon dispersion curve of c-AlN, Spatial component of phonon mode is a-AlN, Energy .vs Time depending on the thickness of amorphous AlN in the composite models, Stress-strain curve, Temperature (T) gradient of the composite model of c-AlN/a-AlN/c-AlN of case 1 and case 2, Heat flux of a-Al_2O_3, a-GaN, a-SiC and a-Si_3N_4. See DOI: 10.1039/x0xx00000x

current. Atomic model of a-AlN was systemically designed by using melt-quenching method. Thin layer of a-AlN shows relatively very small increase in thermal resistance (TR) than c-AlN. we examined that phonon of a-AlN consist of mainly diffuson with good short range of thermal transport. The diffuson is main thermal contributior for good thermal transport of thin a-AlN.

In addition, we also confirmed that thin amorphous structure would be the thermal bridge at the interface. Thermal transport of the composite models of c-AlN/a-AlN/c-AlN was also examined depending on the thickness of a-AlN shows good thermal transference from one to another via thin a-AlN without huge thermal loss. In addition, the phonon properties of amorphous phase for other materials (e.g., Al_2O_3, GaN, SiC and Si_3N_4) also were examined, and the amorphous thin layers indicated high potentials as the thermal bridge that can be used in hetero multilayers of semiconductors. Therefore, the results of tactical design and understanding of the amorphous thin layer at interface can provide insights into the development of promising thermal transport system.

Result and discussion

The models of crystal AlN (c-AlN) and amorphous AlN (a-AlN) of 1.5 nm thickness were prepared (Figure 1). Figure 1c shows the thermal resistances (TRs) of c-AlN and a-AlN. a-AlN just have 3.76 time higher TR than c-AlN. It was known that amorphous phase usually 100 times lower thermal conductivity than crystal phase. However, the thin a-AlN indicates substantially low increase in TR unlike the conventional understanding. Although, NEGF and DFT method, which are introduced to analyze TR, have a size limit in area normal to heat flux by expensive computational cost, the size of 4 unit cells is known to be reliable for NEGF in AlN.[23] Considering the computational cost and reliability for NEGF, 4 unit cell normal to thermal direction was introduced in our models. In addition, AlN film deposited on the hetero-structured substrate has thin amorphous layer at the interface.[15,16] The structural high distortion from incoherency at the interface between different mass and atomic structures would induced thin amorphous transition region at the interface. Therefore, the thin layer of a-AlN might have definite effects on thermal conduction at the interface, and then the mechanism and role of thin amorphous layer have to be scrutinized more closely.

To analyze the fundamental thermal characteristics of amorphous phase, we examined the phonon modes and frequencies for thermal vibrations of c-AlN and a- AlN by using the lattice dynamics (LD). Figure 2a and 2b show the expanded atomic models of c-AlN and a- AlN. The participation ratio ($\mathbf{PR}_n$) was calculated to quantify phonon modes affecting thermal transport. According to the size of the $\mathbf{PR}_n$, phonon modes are normarlly subdivided into propagating phonon (propagon, $\mathbf{PR}_n \geq 0.7$), diffusive phonon (diffuson, $0.7 \geq \mathbf{PR}_n \geq 0.3$) and localized phonon (locon, $\mathbf{PR}_n \leq 0.3$).[32] Figure 2c shows that the most values of $\mathbf{PR}_n$ are higher than 0.5, and particularly $\mathbf{PR}_n$ has higher values than 0.7 in the region of frequency (< 10 THz). It means that transverse acoustic (TA) phonon modes of c-AlN mainly consist of propagon, transferring heat over

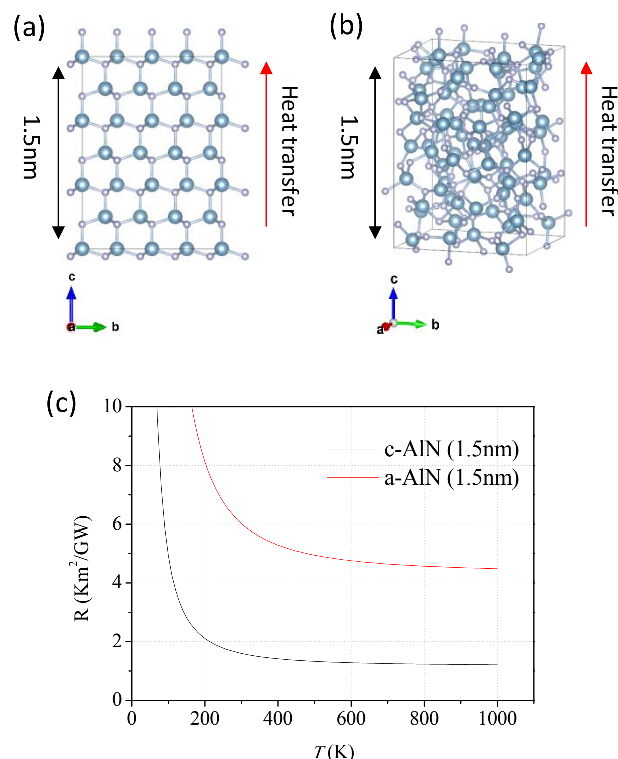

Fig. 1 Atomic structures of (a) c-AlN and (b) a-AlN for thermal NEGF. (c) Thermal resistances (TRs) of c-AlN and a-AlN.

the long distance by long wavelength. There is also gap between 16.8 THz and 18.8 THz. To clarify the gap of $\mathbf{PR}_n$, the phonon dispersion of c-AlN was calculated (Figure S2). The phonon dispersion also has the forbidden region in the similar frequency ranges of $\mathbf{PR}_n$. It is inferred that the gap of $\mathbf{PR}_n$ comes from the forbidden phonon dispersion and also the $\mathbf{PR}_n$ is the reliable. In addition, $\mathbf{PR}_n$ in optical branch of phonon also consist of mainly propagon. It means that phonon modes of c-AlN are mostly propagon in overall frequency region. it is also inferred that c-AlN is beneficial for long range thermal conduction due to large portion of propagon, carrying the heat by sinusoidal vibration of group velocity. However, a-AlN has mostly small values of $\mathbf{PR}_n$ less than 0.7 and the values generally smaller than c-AlN (Figure 2d). In addition, PR_n of a-AlN keeps mostly values higher than 0.3 up to ~23THz, while small portion of PR_n of a-AlN reduces below 0.3 after ~23THz. It means that phonon modes of a-AlN are mostly composed of diffuson that can transfer heat locally within diffusion length.

In addition, normalized thermal conductivity (TC) accumulation was examined by using Green Kubo modal analysis (GKMA) to confirm quantitatively the contributions of diffuson to thermal conduction (Figure 3a).[33] Figure 3a shows that thermal conductivity begins to increase distinctly after 2.63 THz, while there are very small values less than 2.63 THz. The thermal conductivity is continuously accumulated and reaches 90% accumulation at 15.1 THz. The accumulation of thermal conductivity finally goes to 99% at 27.3 THz. Considering that the $\mathbf{PR}_n$ of a-AlN is in diffuson up to 23THz, the accumulation of thermal conductivity in a-AlN by diffuson is 98%, while locon takes 2% for thermal contribution. It means that thermal transport of a-AlN mainly originates from diffuson. To examine specific thermal mechanism of diffuson in a-AlN, we also analyzed

This journal is © The Royal Society of Chemistry 20xx

Please do not adjust margins

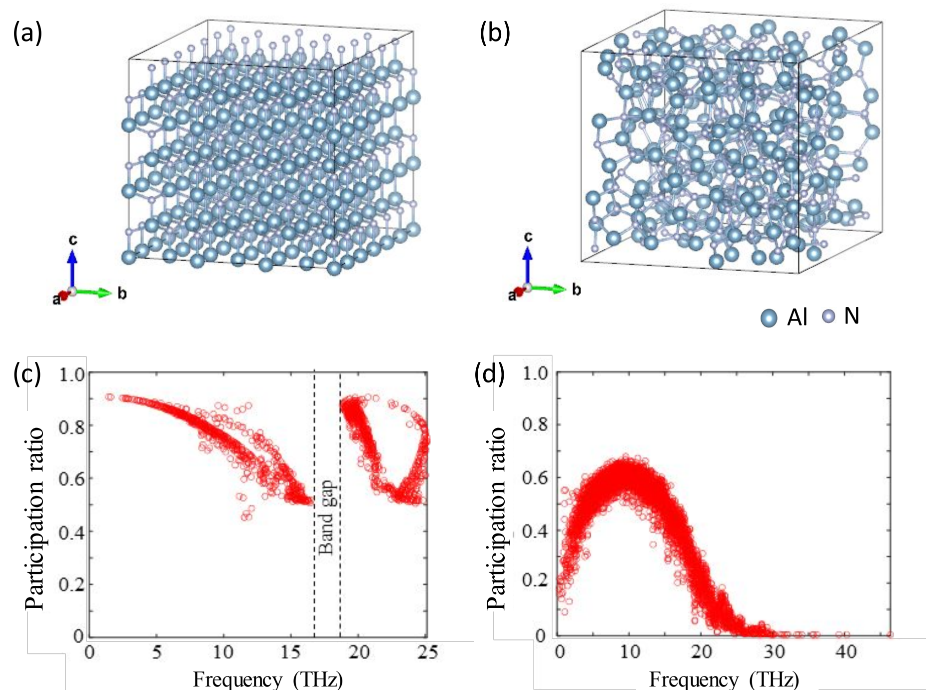

Fig. 2 Atomic structure and participation ratio of (a, c) crystal AlN and (b, d) amorphous AlN.

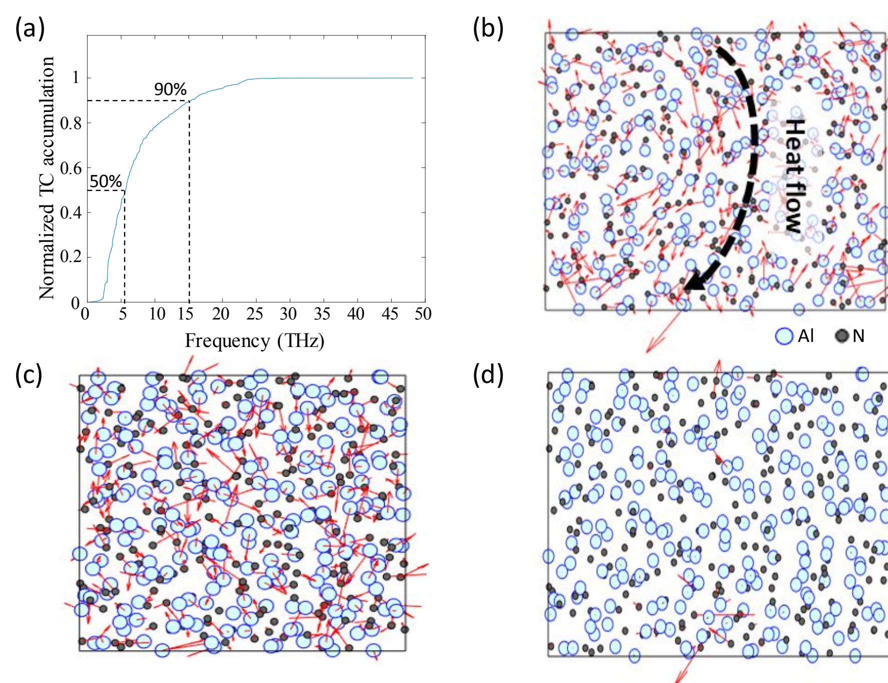

Fig. 3 (a) Normalized thermal conductivity (TC) accumulation of a-AlN. Spatial components of the two-dimensional phonon modes for (b) 2.63 THz, (c) 15.1 THz and (d) 27.3 THz in a-AlN. (Red arrow shows the preferred direction and relative magnitude of phonon modes and black arrow means directions of heat flux.)

the spatial component of phonon modes by clarifying the pictures of vibrational motions at different frequency of a-AlN. Figure 3b and 3c indicate that diffuson can have directional flow at the early frequency of 2.63 THz and sizable vibrations of all atoms at 15.1 THz, facilitating regional thermal transport. It means that diffuson has collective vibration in the media that would carry the heat within their vibration range. However, phonons just vibrate in specific point at 27.3 THz, indicating that locon cannot contribute to thermal transport. Considering that thermal transport of a-AlN is mainly conducted by diffuson with sizable thermal vibration, it is inferred that a-AlN has the potential that can transfer heat well in the short distance within diffusion length of diffusons.

To quantify the diffusion length of phonon modes of a-AlN, phonon mean free path (MFP) was investigated from the spectral decomposed heat current methodology. The spectral heat flux (q) was examined depending on the system length (L). Figure 4a and 4b show the atomic model of a-AlN and heat flux. Heat flux has length

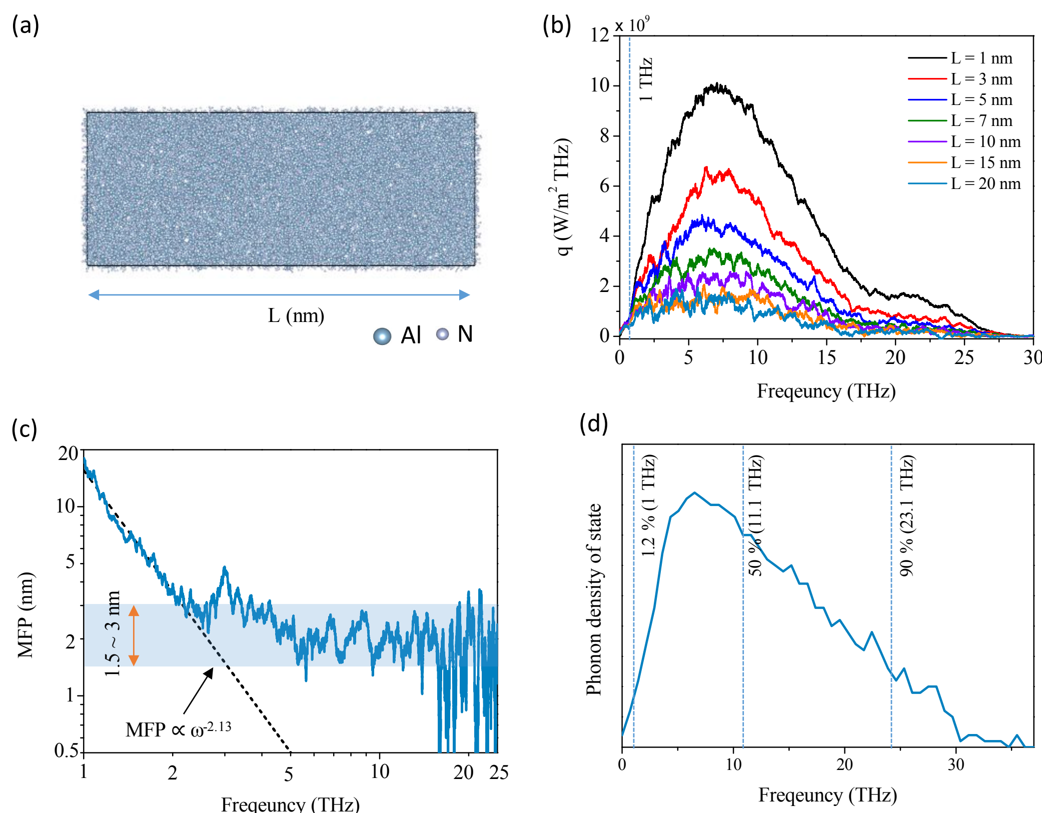

Fig. 4 (a) Atomic model and (b) Heat flux (q) of a-AlN with the different thickness. (c) Mean free path (MFP) and (d) phonon density of state of a-AlN.

dependence in the system. Heat flux is reduced by increase in system length due to strengthening phonon-phonon scattering in the whole range of frequency. However, heat flux is maintained until 1 THz regardless of system length, though the size of heat flux is very small. To examine the thermal mechanism less than 1 THz, spatial components of phonon mode less than 1 THz was also analyzed. Figure S3 shows that atoms have grouped vibration with same directions, indicating group velocity. It means that ballistic transport, indicating that MFP is longer than the introduced system sizes, would happen even in a-AlN at very low frequency, even though its contribution on total heat transport is very small. In addition, at the high frequency, heat flux is substantially reduced because locon at high frequency has difficulty to transport heat. This trend corresponds to $\mathbf{PR}_{\boldsymbol{n}}$ and the normalized TC accumulation.

Figure 4c shows MFP of a-AlN, which obey power law scaling MFP ∝ $\omega^{-2.13}$ below 2.5 THz of modal life time calculation.[14] MFP has the local maximum of 5nm at 3THz, and there is relatively high fluctuation at high frequency due to the sensitivity of heat flux to system sizes. However, MFP has normally mean values of 1.5~3 nm. In addition, figure 4d indicates phonon density of state (PDOS) of a-AlN. The phonon of ballistic conduction below 1THz account for 1.2 %. The PDOS reaches 50 % and 90 % at 11.1Thz and 23.1THz respectively. Although there is small non-zero value at 0 THz due to imaginary part of soft phonon mode, it would be reliable to describe the relative portion of phonon density in the full range of the frequency because the effect of soft phonon is concentrated close to 0 THz. As described in the heat flux, below 1THz, MFP indicates long conduction by ballistic transport over than the maximum system length of 20 nm. However, the phonon contribution to thermal conduction would be very small due to the small density of 1.2 %, even though MFP is relatively very long. It is the reason that normalized TC accumulation is very low at the region of initial frequency. PDOS exhibits that the large portion of the density of ~ 90% is in the diffuson frequency. It means that most phonons of a-AlN are diffuson and have 1.5~3 nm diffusion length on average. Although there is also 8% locon, the thermal contribution is insignificant due to substantially low heat current as shown in figure 3a. Therefore, a-AlN would have very good diffusive thermal conductivity within 1.5~3nm distance by diffuson as reported in the thin amorphous layer at the interface between c-AlN and substrates, indicating the fairly high thermal conductivity compared to bulk c-AlN.[40]

In addition, amorphous layer can have structurally good compatibility with crystalline structures, while the interface of different crystal structures induces large strain, generating large phonon scattering.[15,23,41-43] In addition, we also examined the mechanical modulus of a-AlN by applying tensile stress to a-AlN model. (Figure S4). Figure S4 shows stress ($\boldsymbol{\sigma}$)-strain ($\boldsymbol{\epsilon}$) curve of a-AlN under the tensile stress. By elastic fitting from the curve, Young's modulus (E) of a-AlN is 100.5 GPa, and the value of a-AlN is much lower than the Young's modulus of c-AlN.[44] It means that a-AlN is soft and flexible, indicating beneficial for increasing compatibility at the interface. Furthermore, Inorganic crystal materials usually also have a sizable band gap of PDOS, while the bandgap in amorphous materials could be reduced or extinction.[17] The two different materials at the interface can have non-overlapped region of PDOS

 This journal is © The Royal Society of Chemistry 20xx

Please do not adjust margins

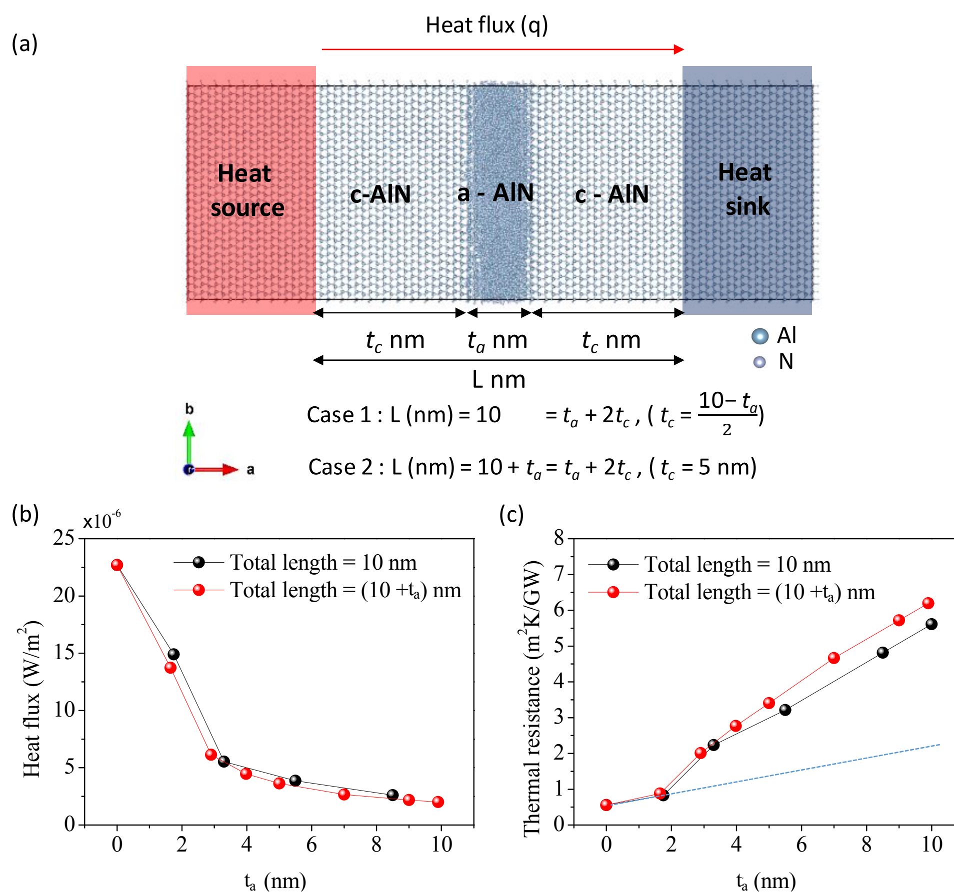

Fig. 5 (a) Atomic structure, (b) Heat flux and (c) thermal resistance of composite models of c-AlN/a-AlN/c-AlN. (Red and blue box are heat source and heat sink respectively. Blue dotted line in figure 5c is the gradient of t=1.77 nm)

and induce phonon incoherency between them, impeding favorable phonon transport for thermal conduction.[45] Filling the non-overlapped region of PODS by introducing amorphous layer would facilitate the phonon transport. In other words, considering the structurally and dynamically compatibility of amorphous structure at the interface, the thin amorphous layer with the diffusive conduction can be considered the reliable thermal bridge at the interface for the composite models.

To validate the reliability of thermal bridge of thin a-AlN layer, the composite model of c-AlN/a-AlN/c-AlN was designed (Figure 5a). To confirm the exact effect of thin amorphous layer on crystalline structure, two cases of fixed total length (10 nm) and length accumulation (10 nm + t_a nm) were prepared. Here, Non-equilibrium molecular dynamics (NEMD) was introduced to examine heat flux by considering anharmonicity for the phonon-phonon scattering.[46] Heat source and heat sink were applied by temperature of 400 K and 200 K respectively for 2,500 ps (Figure S5). The heat flux flows from the heat source to the heat sink in the composite models as the thickness of amorphous AlN layer changes. The case 1 shows that temperature linearly decreases at pure c-AlN and pure a-AlN (Figure S6a and S6g). In addition, the composite models of c-AlN/a-AlN/c-AlN show more distinct decrease in temperature at the a-AlN compared to the both ends of c-AlN, indicating a-AlN introduced at the interface of crystal materials might be relatively thermal barrier (Figure S6).

Figure 5b and 5c indicate heat flux and thermal resistance of the composite models depending on the thickness of a-AlN. the pure c-AlN has highest heat flux and the composite models generally have very low heat flux. However, the heat flux of composite models with t_a =1.77 nm fairly high heat flux compared to the composite models with a-AlN of thickness above 3 nm. It is inferred that thin layer of a-AlN can deliver the heat well within 3nm as the thermal bridge at the interface of two crystal models. Furthermore, the thin thickness of 3nm matches with the average range of MFP of a-AlN, which is mainly contributed by diffusive thermal transport of diffuson. Thermal resistances of the composite models also indicate very mild increase in the a- AlN of t_a =1.77 nm, while the thermal resistances of a-AlN with thickness above 3 nm highly increase (Figure 5c). The extrapolation line of thermal resistance for the composite models with the a- AlN of t_a =1.77 nm is substantially lower than the composite models with more thicker a-AlN above 3 nm.

Furthermore, the heat flux of composite models of case 2 also similar trend in Temperature gradient, heat flux and thermal resistance (Figure S7 and 5). In particular, the heat flux and thermal resistance are almost same with case 1 below the 3 nm thickness of a-AlN. However, decrease in heat flux and increase in thermal resistance of case 2 are distinct above 3nm compared to the thinner a-AlN below 3nm. However, the gradient of thermal resistance of case 2 is similar with case 1 above the 3 nm thickness of a-AlN, though the size of thermal resistance of case 2 slightly increases compared to case 1 above 3nm thickness of a-AlN due to the increase in phonon scattering in longer crystal of case 2 region than case 1. In addition, The heat flux and thermal resistance of two cases are not much different even at t_a=10nm where case 2 has 2 × longer total

Please do not adjust margins

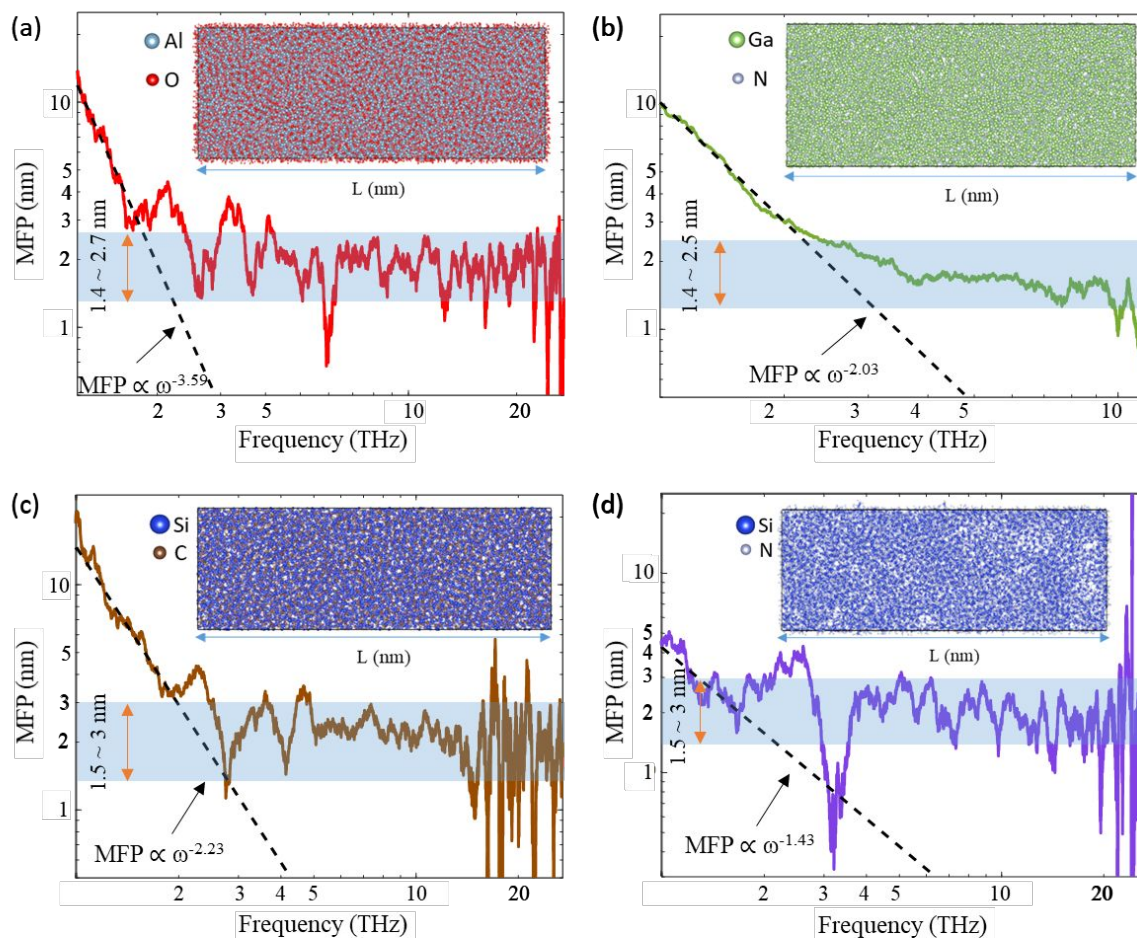

Fig. 6 Mean free path (MFP) of (a) a-Al_2O_3, (b) a-GaN, (c) a-SiC and (d) a-Si_3N_4. (Inset figures are atomic structures.)

model distance compared to case 1. To examine the effect of c-AlN on thermal transport at the two cases, heat flux and mean free path of c-AlN (Figure S8). Although our system of c-AlN might underestimate heat transport compared to crystalline AlN materials with size of micrometers because the maximum size of our c-AlN model was limited to 200 nm, it would be considered reasonable to describe our composite models, considering that the maximum composite length of 20 nm is much shorter than 200nm. Heat flux is transferred dominantly by propagon within 2.2 THz, because heat flux is almost same regardless of the length. Heat flux overall decreases as the length increases. However, heat flux of 10 nm and 20 nm are very close even after 2.2 THz, indicating that heat of c-AlN can be similarly transferred within 20 nm. In addition, mean free path of c-AlN shows tens of nanometers much larger than a-AlN. It is inferred that c-AlN can transfer heat very similarly within 10 nm that is the maximum additional c-AlN region of case 2 compared to case 1. In other words, thermal effect of c-AlN on the thermal resistance is very small compared to a-AlN less than 20 nm that is the maximum size of case 2. Therefore, two composite cases having different length of c-AlN can have similar heat flux and thermal boundary, even though case 2 has the additional c-AlN regions up to 10nm. From the results, it is inferred that the thin amorphous layer diffusively transports the heat regardless of size of crystal structures. Therefore, it means that the thin amorphous layer can conduct comparably the heat delivery within the its diffusion length as thermal bridge for composite models.

To confirm the reliability of application for the thin amorphous layer as thermal bridge, the other electronic materials (e.g., Al_2O_3, GaN, SiC and Si_3N_4), which are extensively used for many electronic applications by forming composite materials, were examined.[14-16] Figure 6 and S9-S12 show the atomic structures and heat flux as the cell length changes of a-Al_2O_3, a-GaN, a-SiC and a-Si_3N_4. Heat flux of all materials have ballistic transportation below 1TH and generally decreases as the cell length increases due to phonon scattering at the most frequency range above 1THz. The heat flux also abruptly decays at the end of the frequency by locon. It means that majority of phonon carrying the heat is the diffuson in these amorphous materials. The trends of the materials are similar to a-AlN. Figure 6 indicates the mean free path of the amorphous materials, and all materials obey the power rule in the early frequency region. In particular, the mean free path of a-Al_2O_3, a-GaN, a-SiC and a-Si_3N_4 are in the mean ranges of 1.4~2.7 nm, 1.4~2.5 nm, 1.5~3 nm and 1.5~3nm respectively. Considering that the main contribution of thermal transport comes from diffusion, these thin amorphous materials could also be considered thermal bridges within the thin thickness of their diffusion lengths by mean free path.

 This journal is © The Royal Society of Chemistry 20xx

Please do not adjust margins

Conclusions

In this study, we fundamentally analyzed the thermal phonon properties of amorphous AlN (a-AlN) and thermal transport via thin amorphous layers at the interface between crystal phases. The most contribution for thermal transport of a-AlN originates from diffuson with on average diffusion length of phonon mean free path of 1.5~3 nm, while contributions of propagon and locon are very small. It means that a-AlN facilitates the short range thermal diffusion within its diffusion length as thin layer. To validate the thermal transport of thin a-AlN layer, thermal transport of the composite models of c-AlN/a-AlN/c-AlN was examined. The composite models of c-AlN/a-AlN/c-AlN show just very small increase in thermal resistance, which is comparable to thermal resistance of pure c-AlN, in the thickness of a-AlN less than 3nm. However, thermal resistance of the composite abruptly increases at the thickness over than 3nm. It means that heat is well transferred without large thermal loss from one to another via amorphous thin layer, and then thin amorphous layer can be considered as thermal bridge at the interface for the composite models. In addition, we also confirm that the other electronic materials (e.g., Al_2O_3, GaN, SiC and Si_3N_4) show also the similar diffusion length of phonon mean free path below 3nm with a-AlN. It means that introduction of thin amorphous layers within the diffusion length of phonon mean free path could be utilized as thermal bridges at interface for various applications of composite materials. This study suggests fundamental mechanism of thermal phonon transport in thin amorphous structures and the promising insight for the design of the thermal transport for application of composite materials.

Experimental

The atomic structures were investigated using DFT method.[20] We utilized spin-polarized generalized gradient approximation parameterized using the Perdew–Burke–Ernzerhof (PBE) exchange correlation functional as implemented in the Vienna Ab Initio Simulation Package (VASP).[21] The cut-off energy for the plane wave basis set was 500 eV for all calculations. Gamma-centered grids 4 × 2 × 1 k-point sampling was used for 2 × 2 × 1 supercell of orthorhombic AlN structure.[22] All structures were fully relaxed to the equilibrium state using the conjugate gradient algorithm.

Thermal resistance of phonon transport was examined by non-equilibrium Green's function (NEGF) formalism, describing the phonon coupling information of the structure, based on the interatomic force constants (IFCs, $\mathbf{\Phi}$) to analyze the thermal resistance of thin layer of crystal (c-AlN) and amorphous AlN (a-AlN).[23-25] Green's function (G), describing the phonon coupling information of the system are introduced as described:[26,27]

$$\mathbf{G(q)} = (\mathbf{I} - \mathbf{D(q)})^{-1} \quad (1)$$

$$\mathbf{D}_{\mu,\upsilon,k,l}(\mathbf{q}) = \frac{1}{\sqrt{M_k M_{k'}}} \sum \mathbf{\Phi}_{\mu,\upsilon}(lk,l'k') e^{iq\cdot R} \quad (2)$$

Where $D_{\mu,\nu,k,l}$ the dynamical matrix of μ and ν directions of *k*th atom in *l*th unit cell, M_k, q and R are the mass of the *k*th atom, the wave number and the lattice vector respectively. From the green's function (G), Phonon transmittance ($\boldsymbol{\zeta}$) are also described as:

$$\boldsymbol{\zeta}(\boldsymbol{\omega}) = \sum_q \mathbf{Tr}[\mathbf{G(q)}\boldsymbol{\Gamma}_L(\boldsymbol{\omega})\mathbf{G(q)}^{\dagger}\boldsymbol{\Gamma}_R(\boldsymbol{\omega})] \quad (3)$$

where $\boldsymbol{\Gamma}_L$ and $\boldsymbol{\Gamma}_R$ are relation for the coupling of left and right ends, $\boldsymbol{\omega}$ is the frequency.[28] Therefore, Heat current ($\boldsymbol{J}$) is evaluated following as:

$$\boldsymbol{J} = \int_0^{\infty} \frac{\hbar\omega}{2\pi} \boldsymbol{\zeta}(\boldsymbol{\omega})[\mathbf{g}(\boldsymbol{\omega},\boldsymbol{T_L}) - \mathbf{g}(\boldsymbol{\omega},\boldsymbol{T_R})]\boldsymbol{d\omega} \cong \Delta\boldsymbol{T} \int_0^{\infty} \frac{\hbar\omega}{2\pi} \boldsymbol{\zeta}(\boldsymbol{\omega}) \frac{\partial \mathbf{g}(\boldsymbol{\omega},\boldsymbol{T})}{\partial \boldsymbol{T}} \boldsymbol{d\omega} \quad (4)$$

where the $\hbar$ and $\mathbf{g}$ are the Dirac constant and Bose-Einstein distribution, T_L and T_R are the temperatures at the left and right ends of the models for calculation of the heat current, respectively, T and ΔT are $(T_L + T_R)/2$ and $|T_L - T_R|$, respectively, and the temperature range introduced was from 0 to 1000 K.[23,28] Therefore, Thermal resistance (TR) and thermal conductance (C) and are derived as

$$\mathbf{TR} = \frac{1}{A}\mathbf{C}^{-1} \quad (5)$$

$$\mathbf{C} = \frac{J}{\Delta T} \approx \int_0^{\infty} \frac{\hbar\omega}{2\pi} \boldsymbol{\zeta}(\boldsymbol{\omega}) \frac{\partial \mathbf{g}(\boldsymbol{\omega},\boldsymbol{T})}{\partial \boldsymbol{T}} \boldsymbol{d\omega} \quad (6)$$

where A is an area that is perpendicular to the heat transport, T is temperature, $\hbar$ and $\mathbf{g}$ are the Dirac constant and Bose-Einstein distribution respectively. The IFCs were examined from the optimized atomic model from DFT and the Green's functions were calculated by ALAMODE.[28]

Phonon eigenmodes were also calculated to investigate the types of phonons in c-AlN and a-AlN consisting of 432 atoms, and then phonon dynamical properties were examined based on the phonon eigenmodes by lattice dynamics trough the general utility lattice program (GULP).[29] In particular, participation ratio ($\mathbf{PR}_n$) was calculated to distinguish phonon modes in c-AlN and a-AlN by using the examined phonon modes and frequency as below:[30-32]

$$\mathbf{PR}_n = \frac{(\sum_i e_{i,n}{}^2)^2}{N \sum_i e_{i,n}{}^4} \quad (7)$$

Where $\boldsymbol{e_{i,n}}$ is the eigenmode for the mode index (n) of i-th atom in the supercell with n atoms.

In addition, Green Kubo modal analysis (GKMA) was utilized to analyze systematically the contribution ($\boldsymbol{k}_{\alpha\beta,\eta\eta'}$) of each phonon mode to thermal conduction as following:[33]

$$\boldsymbol{k}_{\alpha\beta,\eta\eta'} = \frac{V}{k_b T^2} \int \left\langle \boldsymbol{Q}_{\alpha,\eta}(\boldsymbol{t}+\boldsymbol{t}')\boldsymbol{Q}_{\beta,\eta'}(\boldsymbol{t}) \right\rangle \mathrm{d}t' \quad (8)$$

where $\left\langle \boldsymbol{Q}_{\alpha,\eta}(\boldsymbol{t}+\boldsymbol{t}')\boldsymbol{Q}_{\beta,\eta'}(\boldsymbol{t}) \right\rangle$ is the heat flux autocorrelation function for component $\boldsymbol{\alpha}$ and $\boldsymbol{\beta}$ of thermal conductive tensor at phonon mode $\boldsymbol{\eta}$ and $\boldsymbol{\eta}'$, V is the system volume, $\boldsymbol{k_b}$ and $\boldsymbol{T}$ are the Boltzmann constant and temperature.

To investigate reliable thermal length of amorphous layers, phonon mean free path was analyzed based on spectrally decomposed heat current method.[34] The heat flux (Q) can be decomposed spectrally as below:

$$\mathbf{Q} = \int_0^{\infty} \frac{d\omega}{2\pi} \boldsymbol{q}(\boldsymbol{\omega}) \quad (9)$$

where $\boldsymbol{q}(\boldsymbol{\omega})$ is spectrally decomposed heat current. This heat flux of the two atoms of i and j are also described as pair wise as following:

$$\mathbf{Q}_{i\to j} = \int_0^{\infty} \frac{d\omega}{2\pi} \mathbf{q}_{i\to j}(\boldsymbol{\omega}) \quad (10)$$

Here, $\mathbf{q}_{i\to j}(\boldsymbol{\omega})$ is calculated from Fourier transformation of the force velocity cross-correlation function.

$$\mathbf{q}_{i\to j}(\boldsymbol{\omega}) = -\frac{2}{t\omega} \sum_{\alpha,\beta\in\{x,y,z\}} \boldsymbol{Im}\left\langle \hat{v}_i^{\alpha}(\omega)^* K_{ij}^{\alpha\beta} \hat{v}_j^{\beta}(\omega) \right\rangle \quad (11)$$

Please do not adjust margins

where, $\hat{\boldsymbol{v}}$ is the discrete Fourier transformation of the atom velocities($\boldsymbol{v}$) for atom species (i and j) and directions ($\boldsymbol{\alpha},\boldsymbol{\beta} \in \{\boldsymbol{x},\boldsymbol{y},\boldsymbol{z}\}$), $\boldsymbol{K}_{ij}^{\alpha\beta}$ is the interatomic force constant derived by total potential energy ($\boldsymbol{U}$) as described:

$$\boldsymbol{K}_{ij}^{\alpha\beta} = \frac{\partial^2 \boldsymbol{U}}{\partial \boldsymbol{u}_i^{\alpha} \partial \boldsymbol{u}_j^{\beta}}\bigg|_{\boldsymbol{u}=\boldsymbol{0}} \quad (12)$$

$$\boldsymbol{U} \approx \sum_{i,j} \sum_{\alpha,\beta} \boldsymbol{u}_i^{\alpha} \boldsymbol{K}_{ij}^{\alpha\beta} \boldsymbol{u}_j^{\beta} \quad (13)$$

where $\boldsymbol{u}$ is the displacement. In particular, the total spectral heat current in designed model with heat flow passing normal to the model area (A) can be obtained by summing over the species pairs as following:

$$\boldsymbol{q}(\boldsymbol{\omega},\boldsymbol{L}) = \frac{1}{A}\sum_i \sum_j \mathbf{q}_{i\rightarrow j}(\boldsymbol{\omega}) \quad (14)$$

The phonon mean free path (MFP) is derived from the spectral heat current as described:

$$\boldsymbol{q}(\boldsymbol{\omega},\boldsymbol{L}) = \boldsymbol{q}^{\mathbf{0}}(\boldsymbol{\omega})/(\mathbf{1} + \frac{L}{2MFP}) \quad (15)$$

where $\boldsymbol{q}^{\mathbf{0}}(\boldsymbol{\omega})$ is the numerical spectral heat current fitted with $\boldsymbol{L}\longrightarrow\mathbf{0}^{+}$. Analysis of GKMA and spectral decomposition was conducted by using the molecular dynamics (MD) through LAMMPS package with time step 1fs.[35] MD was calculated by Vashishta potential for AlN, Al_2O_3, SiC and Si_3N_4 and Stillinger–Weber potential for GaN.[36-39] All of the amorphous structures were built by melt-quenching method (Figure. S1).[36] The densities of amorphous AlN, Al_2O_3, SiC, Si_3N_4 and GaN are 2.82, 3.48, 2.41, 2.52 and 5.64 g/cm^3 respectively, indicating reliable values close to previous reports.[46-49] Ab initio molecular dynamics (AIMD) was introduced to construct amorphous structure by DTF. AIMD and MD introduced the canonical ensemble (NVT) and NPT ensembles respectively for simplicity of calculation. The crystal structures were initially melted at 3,500 K for 500 ps and then quenched to 10K by the rate of 200K/ps. The quenched structures were equilibrated at 300 K for 200 ps.

Author Contributions

T. Hwang organized and conducted the research, and wrote the manuscript. K. Cho guided all aspects of the work.

Conflicts of interest

There are no conflicts to declare.

Acknowledgements

This work was supported by DARPA Sponsored Special Project.

References

1 E. Pop, *Nano Research*, 2010, **3**, 147-169.
2 Y. Fu, J. Hansson, Y. Liu, S. Chen, A. Zehri, M. K. Samani, N. Wang, Y. Ni, Y. Zhang, Z.-B. Zhang, Q. Wang, M. Li, H. Lu, M. Sledzinska, C. M. S. Torres, S. Volz, A. A. Balandin, X. Xu and J. Liu, *2D Materials*, 2019, **7**.
3 E. Pop, V. Varshney and A. K. Roy, *MRS Bulletin*, 2012, **37**, 1273-1281.
4 Ç. Köroğlu and E. Pop, *IEEE Electron Device Letters*, 2023, **44**, 496-499.
5 S. K. Oh, J. S. Lundh, S. Shervin, B. Chatterjee, D. K. Lee, S. Choi, J. S. Kwak and J.-H. Ryou, *Journal of Electronic Packaging*, 2019, **141**.
6 E. Pop, S. Sinha and K. E. Goodson, *Proceedings of the IEEE*, 2006, **94**, 1587-1601.
7 J. Xu, W.-Y. Yin and J. Mao, *IEEE Microwave and Wireless Components Letters*, 2007, **17**, 55-57.
8 E. Wyrwas, L, Condra, A. Hava, *IPC APEX EXPO Technical Conference*, 2011, 1776–1815.
9 A. Giri, P.E., Hopkins, *Nat Mater*, 2020, **19**, 482-484.
10 L. La Spina, E. Iborra, H. Schellevis, M. Clement, J. Olivares and L. K. Nanver, *Solid-State Electronics*, 2008, **52**, 1359-1363.
11 R. L. Xu, M. Muñoz Rojo, S. M. Islam, A. Sood, B. Vareskic, A. Katre, N. Mingo, K. E. Goodson, H. G. Xing, D. Jena and E. Pop, *Journal of Applied Physics*, 2019, **126**.
12 T. Ozaki, K. Nishio and H. Kino, *Physical Review B*, 2010, **81**.
13 J. Li, K. B. Nam, M. L. Nakarmi, J. Y. Lin, H. X. Jiang, *Appl. Phys. Lett*, 2003, **83**, 5163-5165.
14 R. Rounds, B. Sarkar, D. Alden, Q. Guo, A. Klump, C. Hartmann, T. Nagashima, R. Kirste, A. Franke, M. Bickermann, Y. Kumagai, Z. Sitar and R. Collazo, *Journal of Applied Physics*, 2018, **123**.
15 B. E. Belkerk, A. Soussou, M. Carette, M. A. Djouadi and Y. Scudeller, *Applied Physics Letters*, 2012, **101**.
16 B. E. Belkerk, S. Bensalem, A. Soussou, M. Carette, H. Al Brithen, M. A. Djouadi and Y. Scudeller, *Applied Physics Letters*, 2014, **105**.
17 M. C. Wingert, J. Zheng, S. Kwon and R. Chen, *Semiconductor Science and Technology*, 2016, **31**.
18 H. R. Seyf, L. Yates, T. L. Bougher, S. Graham, B. A. Cola, T. Detchprohm, M.-H. Ji, J. Kim, R. Dupuis, W. Lv and A. Henry, *npj Computational Materials*, 2017, **3**.
19 W. Lv and A. Henry, *Sci Rep*, 2016, **6**, 35720.
20 G. Kresse, J. Furthmiiller, *Computufional Murerials Science* , 1996, **6**, 15-55.
21 J. P. Perdew, K. Burke, M. Ernzerhof, *Phys. Rev. Lett.* , 1996, **77**.
22 Y. Cui, T. Koyama, I. Ohnuma, K. Oikawa, R. Kainuma and K. Ishida, *Acta Materialia*, 2007, **55**, 233-241.
23 C. A. Polanco and L. Lindsay, *Physical Review B*, 2019, **99**.
24 R. Mao, B. D. Kong, C. Gong, S. Xu, T. Jayasekera, K. Cho and K. W. Kim, *Physical Review B*, 2013, **87**.
25 T. Tadano, Y. Gohda and S. Tsuneyuki, *J Phys Condens Matter*, 2014, **26**, 225402.
26 M. Feneberg, R. A. R. Leute, B. Neuschl, K. Thonke and M. Bickermann, *Physical Review B*, 2010, **82**.
27 T. Yamamoto and K. Watanabe, *Phys Rev Lett*, 2006, **96**, 255503.
28 T. Tadano, Y. Gohda and S. Tsuneyuki, *J Phys Condens Matter*, 2014, **26**, 225402.
29 J. D. Gale and A. L. Rohl, *Molecular Simulation*, 2003, **29**, 291-341.
30 H. R. Seyf, W. Lv, A. Rohskopf and A. Henry, *Sci Rep*, 2018, **8**, 2627.
31 C. Lin, D. F. Kelley, M. Rico, A. M. Kelley, *ACS Nano*, 2014, **8**, 3928– 3938.
32 P. Norouzzadeh, C. W. Myles and D. Vashaee, *Physical Review B*, 2017, **95**.
33 H. R. Seyf, K. Gordiz, F. DeAngelis and A. Henry, *Journal of Applied Physics*, 2019, **125**.
34 K. Sääskilahti, J. Oksanen, J. Tulkki, A. J. H. McGaughey and S. Volz, *AIP Advances*, 2016, **6**.
35 P. Thompson, H. M. Aktulga, R. Berger, D. S. Bolintineanu, W. M. Brown, P. S. Crozier, P. J. in 't Veld, A. Kohlmeyer, S. G.

This journal is © The Royal Society of Chemistry 20xx

Please do not adjust margins

Moore, T. D. Nguyen, R. Shan, M. J. Stevens, J. Tranchida, C. Trott, S. J. Plimpton, *Comp Phys Comm*, 2022, **271**, 10817.
36 H. Xiang, H. Li and X. Peng, *Computational Materials Science*, 2017, **140**, 113-120.
37 Q, Xu, N. Salles, J. Chevalier, J. Amodeo, *Modelling Simul. Mater. Sci. Eng*, 2022, **30,** 035008.
38 A. Béré and A. Serra, *Philosophical Magazine*, 2006, **86**, 2159-2192.
39 P. Vashishta, R. K. Kalia, A. Nakano, J. P. Rino, *J. Appl. Phys.*,2007, **101**, 103515.
40 A. Dasmahapatra and P. Kroll, *Computational Materials Science*, 2018, **148**, 165-175.
41 X. Wu, P. Yang, C. Li and Q. Han, *International Journal of Heat and Mass Transfer*, 2023, **201**, 123643.
42 C-C. Chou, J-S. Lin and R. Wu, *Ceramics International*, 2017, **43**, S776–S783.
43 Ł. Kaczmarek, A. Kyzioł, D. Kottfer, W. Szymanski, K, Kleszcz and K. Kyzioł, Appl. Phys. 2014, **115**, 014901.
44 I. Yonenaga, T. Shima and M. H. F. Sluiter, *Jpn. J. Appl. Phys.*, 2002, **41**, 4620-4621.
45 C. Perez, A. J. McLeod, M. E. Chen, S. I. Yi, S. Vaziri, R. Hood, S. T. Ueda, X. Bao, M. Asheghi, W. Park, A. A. Talin, S. Kumar, E. Pop, A. C. Kummel and K. E. Goodson, *ACS Nano*, 2023, **17**, 21240-21250.
46 X. Wu and T. Luo, *J. Appl. Phys.*, 2014, **115**, 014901.
47 Y. Zhao, X. Peng, T. Fu, C. Huang, H Xiang, N. Hu and Cheng Yan, *Materialia*, 2018, **2**, 148-156
48 C. Århammar, A. Pietzsch, N. Bock, E, Holmström, C. M. Araujo, J. Gråsjög, S. Zhaog, S. Green, T. Peery, F. Hennies, S. Amerioun, A. Föhlisch, J. Schlappa, T. Schmitt, V. N. Strocov, G. A. Niklasson, D. C. Wallace, J-E Rubensson, B. Johansson and R. Ahuja, *PNAS*, 2011, **108**, 6355–6360.
49 Y. Y. Kim, *Materials*, 2022, **15**, 2165.
50 Y. Pan, Y. Liu, P. Wang, X. Qi, R. Li, D. Yin and J. Yao, *Journal of Non-Crystalline Solids*, **2024**, 633, 122965.
51 B. Cai and D. A. Drabold *Physical Review B*, 2013, **87**. 075216.

This journal is © The Royal Society of Chemistry 20xx

Please do not adjust margins

The data supporting this article have been included as part of the article and ESI, and are available upon reasonable requests.